19th Brazilian Congress of Thermal Sciences and Engineering
November 6th–10th, 2022, Bento Gonçalves - RS - Brazil

ENC-2022-0480
FERROFLUID DROPLETS UNDER EXTERNAL MAGNETIC FIELD AND SHEAR FLOW IN NON-EQUILIBRIUM MAGNETIZATION REGIME

Arthur L. Guilherme
Taygoara F. de Oliveira
Department of Mechanical Engineering - Universidade de Brasília, Brasília, DF 70910-900, Brazil
arthur.guilherme@aluno.unb.br
taygoara@unb.br

Abstract. *Ferrofluid droplets immersed in a non-magnetizable carrier fluid subjected to the combined action of a simple shear flow and external magnetic fields are studied in this work. This problem has potential applications in areas such as microfluidics, biomedicine, and microrheology and has been subject of research recently. Nevertheless, up to our knowledge all theoretical and numerical studies consider superparamagnetic ferrofluids, i.e. the local magnetization is linearly proportional to the local magnetic field. In the present work, we consider the regime of non-equilibrium magnetization, in which the local magnetization is influenced by the vorticity, brownian magnetic relaxation and precessional magnetic torque, as described by the Shliomis (1971) model. The non-dimensional parameters governing the problem are the Péclet number (Pe), accounting for the ratio between brownian relaxation time and a characteristic time of the shear flow; the capillary number (Ca), which is the ratio between shear stress and surface tension; and a magnetic capillary number (Ca_{mag}), that measures the ratio between magnetic stress and surface tension. The three-dimensional problem has a full set of fifteen well-coupled equations. They are the incompressible Navier-Stokes with interface and magnetic forces source terms, Maxwell's equations at magnetostatic limit, the magnetization evolution equation, the equilibrium magnetization equation and the interface capturing equation. The classical projection method is used to solve the pressure-velocity coupling. The finite-difference in a staggered grid is used to discretize space. The time integration is made through a Crank-Nicolson scheme for the momentum equations and the explicit Euler method for the magnetization evolution. The interface capturing problem is treated using a level-set method with conservative high-order time and space discretization. We present results comparing the bulk and local magnetization, droplet deformation, and susceptibility behavior for different Pe at distinct flow conditions, i.e., distinct Ca and Ca_{mag} and distinct magnetization regimes. It was observed that vorticity could change the monotonicity of the bulk magnetization and deformation with respect to Pe_m.*

Keywords: *Magnetization, Ferrofluid droplet, Magnetic relaxation, Level set method*

1. INTRODUCTION

The application of uniform magnetic fields on a ferrofluid droplet immersed in a non-magnetizable quiescent carrier fluid induces forces that lead to the deformation of the droplet in the direction of the applied magnetic field. When the droplet is also subjected to an external flow, the droplet configuration becomes a function of the viscous, magnetic and interfacial forces acting on it. Several theoretical, experimental and numerical works focusing on this problem have been published in recent years. They range from micro applications point of view of droplet configuration and breakup analysis (Cunha *et al.*, 2018) to the macro magnetic emulsions rheology and magnetization properties studies (Cunha *et al.*, 2020; Ishida and Matsunaga, 2020; Abicalil *et al.*, 2021; Capobianchi *et al.*, 2021).

Ferrofluid liquids are composed of colloidal suspensions of magnetic particles suspended in some non-magnetizable liquid. The equilibrium magnetization of such fluids obeys a Langevin dynamic response to the local magnetic field, in the way that at low applied magnetic fields the magnetization grows linearly with the local magnetic field and then saturates in the limit of high fields. When vorticity plays an important role in rotating the magnetic particles, a non-equilibrium magnetization which is function of the magnetic time scales of the particles arises (Shliomis *et al.*, 1971).

Up to our knowledge, although there are numerical and theoretical studies of ferrofluid droplets that account for Langevin dynamics, i.e., with the magnetic susceptibility as a function of the local magnetic field (Zhu *et al.*, 2011; Rowghanian *et al.*, 2016), and there are studies on the effects of the magnetic relaxation on ferrofluid flows (de Carvalho and Gontijo, 2020; Yang and Liu, 2020), there is no numerical or theoretical study of ferrofluid droplets that consider the

influence of the vorticity on the orientation of the magnetization.

In this work, we model our ferrofluid droplet based on the non-equilibrium regime. For this the phenomenological evolution equation of Shliomis *et al.* (1971) for the magnetization field is implemented, as shown in Section 2. In the same section, we explain the coupled magnetic-hydrodynamic physics of the problem. In Section 3.we expose the numerical settings. Then, in Section 4.we show the results of that investigation, which begins by exploring an equilibrium Langevin situation and moves toward the non-equilibrium one. Finally, in Section 5.we make our conclusions and considerations for future works.

2. PROBLEM STATEMENT

The problem under study is that of a single ferrofluid droplet of radius a immersed in a non-magnetizable carrier fluid of same density ρ and viscosity η and subjected to simple shear flow and an external magnetic field in a three-dimensional domain. The imposed shear rate is $\dot{\gamma} = 2U/L_y$, where L_y is the length of the domain in the y-direction (the same for L_x and L_z) and U is the velocity in the x-direction applied in the y planes boundaries. The magnetic field is applied with intensity H_0 in the y-direction, as sketched in Fig. 1. Both shear and magnetic forces induce deformation of the droplet of magnetic susceptibility χ and interface tension coefficient σ, which responds with restorative capillary forces. The vorticity ξ which is inherent in shear flow and is transmitted from the external flow to inside the droplet rotates the magnetization $\mathbf{M}$ with respect to the local magnetic field $\mathbf{H}$ if the magnetic relaxation time of the magnetic particles present in the ferrofluid (τ_R, see later in this section) is not rapid enough to align the magnetization with the magnetic field, i.e, in the situation of non-equilibrium magnetization.

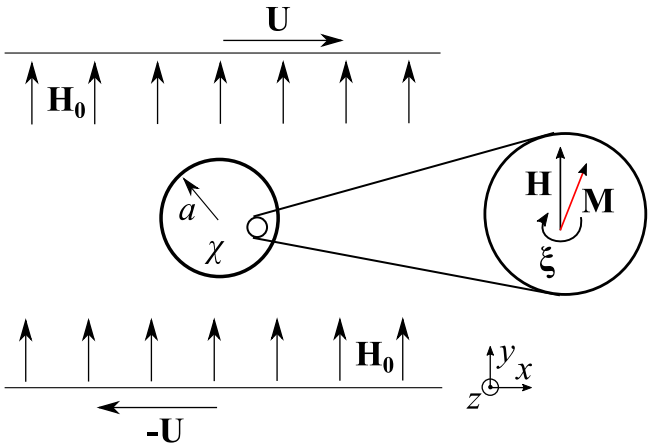

Figure 1. Sketch of the problem.

The problem has thus two natures of interacting physics. The electromagnetics and the hydrodynamics. The Maxwell's equations at the magnetostatic limit are (Rosensweig, 2013):

$$\nabla \cdot \mathbf{B} = \mathbf{0}, \quad \text{and} \quad \nabla \times \mathbf{H} = \mathbf{0} \tag{1}$$

Where $\mathbf{B}$ is the magnetic induction which is associated with the magnetic field $\mathbf{H}$ and the magnetization $\mathbf{M}$ through $\mathbf{B} = \mu_0(\mathbf{H} + \mathbf{M})$, where μ_0 is the magnetic permeability of the free space. As the magnetic field is irrotational, it can be described as the gradient of a scalar field, the magnetic potential $\nabla\psi = -\mathbf{H}$. Replacing these expressions onto Eq. (1), we get the following Poisson's equation for magnetic potential.

$$\nabla^2\psi = \nabla \cdot \mathbf{M} \tag{2}$$

If we assume, however, an equilibrium regime for the magnetization, i.e, there is no misalignment between the local magnetic field and magnetization, we can relate the magnetization and the local magnetic field through the co-linear relation $\mathbf{M} = \chi\mathbf{H}$, where χ is the local magnetic susceptibility. We can define thus a continuous function $\zeta(\mathbf{x}) = 1+\chi(\mathbf{x})$. Therefore, we have the following Poisson's equation for the magnetic potential in the equilibrium regime of magnetization:

$$\nabla \cdot (\zeta(\mathbf{x})\nabla\psi) = 0 \tag{3}$$

This function is equal to the unit in the matrix fluid and is a property, greater than one, of the ferrofluid. Inside the droplet, it can be considered either a constant or a function of the local magnetic field. The magnetization of ferrofluids

with a small volume fraction of equal-sized magnetic particles responds to the applied magnetic field through the Langevin dynamics that gives the relation (Shliomis *et al.*, 1971):

$$\mathbf{M_0} = nm\mathcal{L}(\alpha)\hat{\mathbf{H}}, \quad \boldsymbol{\alpha} = \frac{\mu_0 m\mathbf{H}}{k_B T} \tag{4}$$

The subscript 0 indicates the equilibrium regime. n is the number of magnetic particles per unit of volume, m is the magnetic dipole strength, k_B is the Boltzmann's constant, T the absolute temperature, and α, a non-dimensional parameter relating the ratio between the magnetic and thermal energies. The function $\mathcal{L}$ is the Langevin function, $\mathcal{L}(\alpha) = cotanh(\alpha) - 1/\alpha$, which saturates at one, so that $M_s = nm$ is the saturation magnetization of the ferrofluid. Therefore we have, for the equilibrium regime, the following expression for ζ (Zhu *et al.*, 2011).

$$\zeta = 1 + \chi = 1 + \frac{M}{H} = 1 + \frac{nm}{H}\mathcal{L}(\alpha) \tag{5}$$

In the non-equilibrium regime, when the vorticity experienced by the magnetic particles becomes significant and tends to rotate the fluid magnetization locally, the Eq. (5) no longer applies. Instead, we have to solve an evolution equation for the magnetization field. Here, we use the phenomenological evolution equation of (Shliomis *et al.*, 1971).

$$\frac{\partial \mathbf{M}}{\partial t} + \mathbf{u}\cdot\nabla\mathbf{M} = \frac{1}{2}\boldsymbol{\xi}\times\mathbf{M} - \frac{1}{\tau_R}(\mathbf{M}-\mathbf{M_0}) - \frac{\mu_0}{6\eta\phi_f}\mathbf{M}\times(\mathbf{M}\times\mathbf{H}) \tag{6}$$

Where t is the time, $\mathbf{u}$ is the velocity field and ϕ_f is the volume fraction of magnetic particles of individual volume V that composes the ferrofluid. Note that $\phi_f = nV$ and the particle magnetization M_d is $M_d = M_s/\phi_f$. The right-hand side is composed of three terms. The first is a source of misalignment caused by flow vorticity. The third one is a precession term, which tends to retain the magnetization in the direction of the magnetic field. The second one is a relaxation term, which relaxes the magnetization toward its equilibrium state in a function of its magnetic relaxation time, τ_R. Here, τ_R is considered to be equal to the brownian relaxation time, i.e., $\tau_R = 3\eta V/k_B T$. Note that the velocity field $\mathbf{u}$ as well as the vorticity ξ are unknown and should be calculated by solving the hydrodynamic equations.

The hydrodynamic problem is governed by the incompressible Navier-Stokes equations with the capillary and magnetic forces, $\mathbf{F_c}$ and $\mathbf{F_m}$, respectively. So that,

$$\rho\left(\frac{\partial\mathbf{u}}{\partial t} + \mathbf{u}\cdot\nabla\mathbf{u}\right) = -\nabla p + \eta\nabla^2\mathbf{u} + \mathbf{F_c} + \mathbf{F_m} \tag{7}$$

$$\nabla\cdot\mathbf{u} = 0 \tag{8}$$

Where p is the pressure. The capillary forces $\mathbf{F_c}$ are computed through the use of the signed distance function ϕ, an element of the level set method further discussed in Section 3.1, which concentrates the force smoothly at the interface (Abicalil *et al.*, 2021):

$$\mathbf{F_c} = -\sigma\kappa\delta(\phi)|\nabla\phi|\hat{\mathbf{n}} \tag{9}$$

where κ is the local mean curvature, δ is the Dirac smooth delta function, and $\hat{\mathbf{n}}$ is the normal vector pointing outward the droplet surface. The magnetic force has two terms, one which corresponds to the Kelvin force and another corresponding to the magnetic torques as follows:

$$\mathbf{F_m} = \mu_0\mathbf{M}\cdot\nabla\mathbf{H} + \frac{\mu_0}{2}\nabla\times\mathbf{M}\times\mathbf{H} \tag{10}$$

Note that in the case of equilibrium regimes, the second term vanishes and the force can be written as $\mathbf{F_m} = \mu_0(\zeta - 1)\mathbf{H}\cdot\nabla\mathbf{H}$.

2.1 Non-dimensional equations

The non-dimensional form of the equations is obtained using the following scales: a for length, $1/\dot{\gamma}$ for time, $\dot{\gamma}a$ for velocity, $\rho\dot{\gamma}^2a^2$ for pressure, and the magnitude of the applied magnetic field H_0 for the magnetic field and the magnetization. Note that the vorticity $\boldsymbol{\xi}$ is scaled with $\dot{\gamma}$.

This scaling leads to the the continuity equation and magnetic potential equations of the same form as Eq. (8), Eq (2) and Eq (3), respectively. All variables are hereafter in the non-dimensional form. Additional symbols are not taken in order to simplify the nomenclature. The Navier-Stokes equations become the following.

$$\frac{\partial \mathbf{u}}{\partial t} + \mathbf{u}\cdot\nabla\mathbf{u} = -\nabla p + \frac{1}{Re}\nabla^2\mathbf{u} - \frac{1}{ReCa}\kappa\delta(\phi)|\nabla\phi|\hat{\mathbf{n}} + \frac{Ca_{mag}}{ReCa}\left(\mathbf{M}\cdot\nabla\mathbf{H} + \frac{1}{2}\nabla\times\mathbf{M}\times\mathbf{H}\right) \tag{11}$$

The magnetization evolution equation, the equilibrium magnetization equation and the equation for $\zeta(\mathbf{x})$ becomes

$$\frac{\partial \mathbf{M}}{\partial t} + \mathbf{u}\cdot\nabla\mathbf{M} = \frac{1}{2}\boldsymbol{\xi}\times\mathbf{M} - \frac{1}{Pe_m}(\mathbf{M}-\mathbf{M_0}) - \frac{Ca_{mag}}{6Ca\phi_f}\mathbf{M}\times(\mathbf{M}\times\mathbf{H}), \tag{12}$$

$$\mathbf{M_0} = \phi_f M_d \mathcal{L}(M_d Pe_m Ca_{mag} H/3Ca) \tag{13}$$

and

$$\zeta(\mathbf{x}) = 1 + \frac{\phi_f M_d}{H}\mathcal{L}(M_d Pe_m Ca_{mag} H/3Ca) \tag{14}$$

The problem is thus dictated by the Equations (8), (11), (12), (13) and (2) for the non-equilibrium regime. And Equations (8), (11), (14) and (3) for the equilibrium Langevin regime. The non-dimensional parameters governing the problem are the Reynolds number $Re = \rho\dot{\gamma}a^2/\eta$, the capillary number $Ca = \eta\dot{\gamma}\eta/\sigma$, the magnetic capillary number $Ca_{mag} = \mu_0 H_0^2 a/\sigma$, the magnetic Peclét number $Pe_m = \tau_R\dot{\gamma}$, the non-dimensional magnetization of magnetic particles $M_d^\star = M_d/H_0$ and the volume fraction of the magnetic particles composing the ferrofluid ϕ_f. The last parameter is a property of the ferrofluid, while the others are parameters of the flow/magnetic field. The Reynolds number is the ratio between inertial and viscous effects at the droplet length scale, the capillary number measures the ratio between the viscous stresses and surface tension restoring force, the capillary magnetic number is the ratio between the magnetic forces acting on the surface and the surface tension, and the magnetic Peclét measures the ratio between the time scales of the browninan relaxation and that of the flow. In other words, the latter measures the degree of the state of non-equilibrium. The evolution equation used in this work does not predict well the behavior of the magnetization for high non-equilibrium situations, being its accuracy limited to $Pe_m \ll 1$ (Shliomis, 2001). Finally, $M_d^\star$ measures the strength of the magnetization compared to the applied magnetic field (the * symbol will not appear hereafter).

3. COMPUTATIONAL SOLUTION

3.1 Level-set method

The interface problem is treated with the well-established Level-Set method, which is already used in numerical studies of ferrofluid droplets (Zhu *et al.*, 2011; Cunha *et al.*, 2018, 2020; Abicalil *et al.*, 2021). This method consists of evolving a signed distance function ϕ, in which the zero level corresponds to the interface between the phases, being the positive values referent to the matrix and the negative values to the droplet. The droplet is initialized as a sphere of radius one so that ϕ is easily distributed throughout the domain. The signed distance function is thus advected with the flow through the advection equation (Sussman *et al.*, 1994):

$$\frac{\partial \phi}{\partial t} + \mathbf{u}\cdot\nabla\phi = 0 \tag{15}$$

The interface can be then captured at any simulation time. The level-set permits a smooth transition of properties between the phases. A small value ϵ is defined to be this narrow band surrounding the interface in which the property varies from one phase to the other, and a smooth Heaviside function H_ϵ is applied (Sussman *et al.*, 1998):

$$H_\epsilon(\phi) = \begin{cases} 0, & \text{if } \phi < -\epsilon, \\ \frac{1}{2}\left[1 + \frac{\phi}{\epsilon} - \frac{1}{\pi}\sin\phi\phi/\epsilon\right], & \text{if } |\phi| \le \epsilon, \\ 1, & \text{if } \phi > \epsilon \end{cases} \tag{16}$$

The corresponding delta function $\delta(\phi)$ is the derivative of H_ϵ with respect to ϕ. The interface thickness is generally chosen to be, as in this work, $\epsilon = 1.5h$ where h is the size of the grid cell. This smooth Heaviside is used for example to

obtain a more spatially general smooth ϕ_f, replacing it by $\phi_{f-general}(\phi) = \phi_f[1 - H_\epsilon(\phi)]$. Although Eq. (15) accurately transports the level zero, i.e., interface, it deviates from the signed distance function along the iterations. Methods for reinitializing ϕ at each time step are implemented in this work, including volume constraints that guarantee the conservation of volume (Sussman and Fatemi, 1999). The conservative level-set approach of Sussman and Fatemi (1999) is used in our code. The reader is referred to Abicalil *et al.* (2021) for a more detailed explanation of the conservative level-set method used in this work including details of the reinitialization process.

3.2 Projection Method

The incompressible Navier-Stokes equations, including the momentum balance and continuity, are solved by using the projection method proposed by (Kim and Moin, 1985). It consists of solving the momentum equation ignoring the pressure field and then projecting this resultant velocity field, $\mathbf{u}^\star$ to the divergence-free vector space. The first step is made by using a semi-implicit Crank-Nicolson scheme to discretize the time and a second-order Adams-Bashforth scheme is used to extrapolate the variables treated explicitly. The following two steps characterize the scheme. For further explanation refer to (Kim and Moin, 1985).

$$\frac{\mathbf{u}^\star - \mathbf{u}^n}{\Delta t} = -(\mathbf{u}\cdot\nabla\mathbf{u})^{n+1/2} + \frac{1}{2Re}\nabla^2(\mathbf{u}^n + \mathbf{u}^\star) + \frac{1}{ReCa}{\mathbf{F_c}}^{n+1/2} + \frac{Ca_{mag}}{ReCa}{\mathbf{F_m}}^{n+1/2} \tag{17}$$

$$\frac{\mathbf{u}^{n+1} - \mathbf{u}^\star}{\Delta t} = -\nabla p_v^{n+1} \tag{18}$$

Where p_v is a virtual pressure. Taking the divergence of the last equation and imposing the incompressibility of $\mathbf{u}^{n+1}$ we get:

$$\nabla^2 p_v^{n+1} = \frac{1}{\Delta t}\nabla\cdot\mathbf{u}^\star \tag{19}$$

Thus, the sequence steps of Equations (17), (19) and (18) define the projection method used to compute the hydrodynamic problem in this work. The boundary conditions for the artificial variables $\mathbf{u}^\star$ and p_v are the same as the respective real ones, i.e., periodic in the x and z-direction and Dirichlet and Neumann in the y-direction for $\mathbf{u}$ and $\mathbf{p}$, respectively.

3.3 Magnetic potential equations

The boundary condition for the Poisson equations for the magnetic potential in equilibrium and non-equilibrium cases is that of uniform applied magnetic field $\mathbf{H_0}$, i.e., the Neumann condition $\nabla\psi = -\mathbf{H_0}$.

3.4 Numerical setting

The spatial discretization is made by using a staggered grid (also called Marker-and-Cell grid) with scalars defined in the cell centers and vector components in their respective cell faces (Kim and Moin, 1985). Second-order finite differences thus are implemented, except for the advection terms of the momentum equation and magnetization evolution which use both a second-order non-oscillatory (ENO) scheme, and the advection term of the level-set equation, which uses a fifth-order weighted non-oscillatory (WENO) scheme (Jiang and Peng, 2000). Poisson's equations are discretized with second-order finite differences. The magnetization equation is integrated in time through the explicit Euler method. Thus, a small time step of $\Delta t = 1e-5$ was used. The domain is of dimensions $10a$ x $10a$ x $7.5a$ for all cases and is discretized in 128 x 128 x 96 nodes for the equilibrium case described in Section 4. but in 152 x 152 x 114 nodes for the non-equilibrium cases in order to capture the small angles of misalignment. For both cases, the domain gives a volume fraction between the droplet and the domain of $\beta = 0.56\%$. All results presented here are steady-state solutions.

4. RESULTS

4.1 Equilibrium regime: Langevin dynamics

First, we analyze the consideration of non-constant χ inside the droplet, still in the equilibrium regime, in order to understand the Langevin dynamics on the bulk magnetization of the system composed of the suspension of a ferrofluid droplet in another quiescent non-magnetizable liquid before we go to the non-equilibrium regime.

As we calculate the magnetization contribution to the magnetic potential either implicitly by using Eq. (14) or by using the magnetization evolution with Euler explicit time integration, this analysis will also serve as a validation for the Euler explicit magnetization evolution.

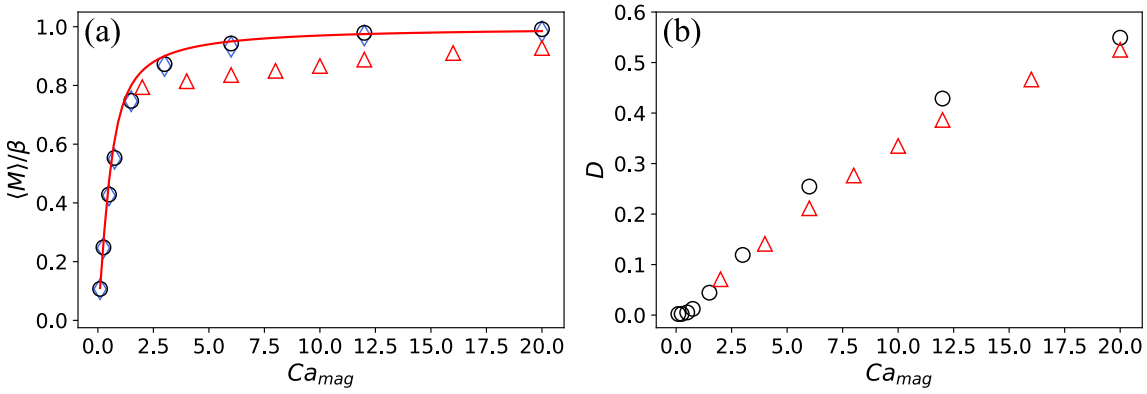

Figure 2. Bulk magnetization normalized with the ratio between the volume of the droplet and the volume of the domain β in function of Ca_{mag} for the implicit approach (black circles) and explicit (blue diamonds) (left). Also in (left) is plotted for reference the case of constant $\chi = 1$ (red triangles) and the Langevin function with same argument as the implicit and explicit approaches and constant $H = 1$ ($M_d = 10$, $\phi_f = 0.1$, $Ca = 0.002$, $Pe_m = 0.002$). And Deformation in function of Ca_{mag} for the implicit approach (black circles) and constant $\chi = 1$ (red triangles).

The bulk magnetization $\langle M \rangle$ (already in non-dimensional form, i.e., scaled by H_0) is the volumetric average of the magnetization on the entire domain and is calculated as follows (Cunha *et al.*, 2020):

$$\langle \mathbf{M} \rangle = \frac{1}{V}\int_V \mathbf{M} dV = \frac{1}{V}\int_V (\zeta - 1)\mathbf{H} dV \tag{20}$$

For this analysis, we set an equilibrium situation and quiescent external liquid by setting a weak nonequilibrium $Pe_m = 0.002$ together with a very weak flow $Ca = 0.002$. $M_d = 10$ and $\phi_f = 0.1$ are used in order to keep the M smaller than H_0. The argument of the Langevin function in Eq. (13) and (14) with theses values indicates that $0.1 \leq Ca_{mag} \leq 20$ is a good band to capture both Langevin and droplet elongation effects on the magnetization. The elongation effect on the magnetization is characterized by the fact that the magnetic field induced at the interior of a droplet under an external uniform magnetic field has an intensity H_{in} smaller than that of the applied field for constants χ, and it becomes closer to the applied value as long as the droplet elongates (Afkhami *et al.*, 2010). This effect of demagnetization is well described in the expression $H_{in} = \mu_{out} H_0/[(1-k)\mu_{out} - k\mu_{in}]$, where μ_{in} and μ_{out} are respectively the permeability in and out the droplet and k is the geometrical demagnetization factor, which has maximum value $k = 1/3$ when the droplet is a sphere (Afkhami *et al.*, 2010).

Figure 2 shows the bulk magnetization and also the deformation measured with the parameter $D = (L-B)/(L+B)$ (known as Taylor deformation) (Taylor, 1934), where L is the major semi-axis and B the minor semi-axis of the droplet, with respect to Ca_{mag} for the equilibrium state calculated from both approaches. For comparison, it is also plotted the results for a fixed magnetic susceptibility $\chi = 1$ (which responds uniquely to the demagnetization effect due to the geometry of the droplet) and the Langevin function for the same parameters and $H = 1$.

The bulk magnetization increases with Ca_{mag} in a non-linear manner. First, it increases very rapidly although the droplet remains almost undeformed ($0.1 \leq Ca_{mag} \leq 1.5$), indicating the most responsible effect for this increase is the linear region of the Langevin at low fields. Here, we recall that the magnetic force which tends to deform the droplet is function of Ca_{mag} and magnetization intensities, on the other hand, the more deformed droplet induces lower demagnetization inside the droplet, which increases the magnetization. Comparing the results with the Langevin function (with H always equal to one) we see the small deviation due to the droplet demagnetization. It becomes more evident in the transition region. In there, however, the droplet starts to elongate. Next in the saturation region, the elongation becomes more pronounced and as a result, the demagnetization drops which approximates the measured bulk magnetization and the Langevin function. As a resume, it is evident that the bulk magnetization is more likely to be a function of the Langevin behavior.

Figure 3 shows an interesting effect of the demagnetization of the droplet. We see that the demagnetization is not only a function of its elongation but also of the susceptibility of the ferrofluid. When Ca_{mag} is too weak, the susceptibility drops and the magnetic field is almost unchanged by the presence of the ferrofluid droplet, leading to lower demagnetizations and higher H_{in}. These additional effects increase the non-linearity of the problem, because the magnetization increases with the susceptibility, but the demagnetization also increases reducing the resulting susceptibility.

These effects induce a non-monotonic behavior of the ferrofluid magnetic susceptibility χ. This behavior is perceived by the direct observation of Fig. 2. By comparison with the curve for $\chi = 1$, we see an increase at low fields, in that case surpassing $\chi = 1$ at $Ca_{mag} \approx 1.5$, reaching a maximum value at $Ca_{mag} \approx 5$, and then it starts to decrease approximating

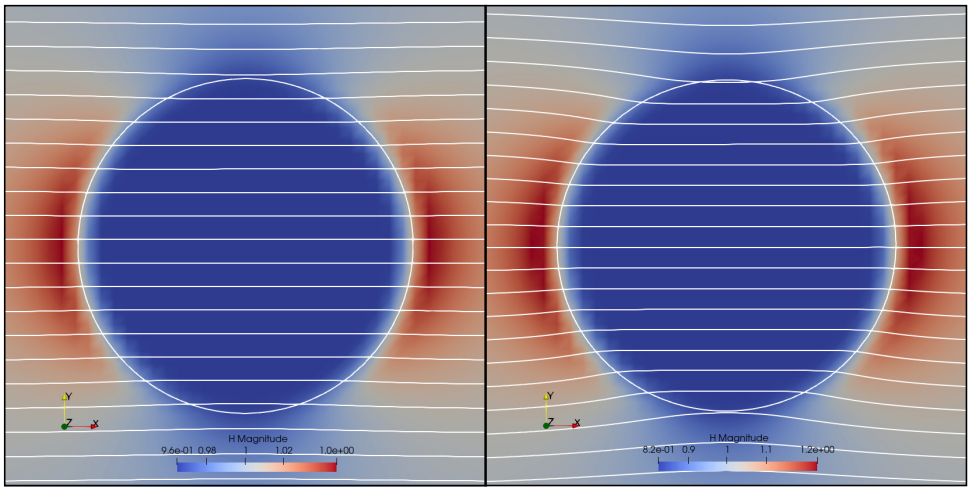

Figure 3. Magnetic field intensity and streamlines inside the almost undeformed droplet for the cases $M_d = 10$, $\phi_f = 0.1$, $Ca = 0.002$, $Pe_m = 0.002$ for two different Ca_{mag}. In the left $Ca_{mag} = 0.1$, in the right $Ca_{mag} = 0.75$.

both curves. The influence of the effects becomes more clear in Fig. 4, which shows χ and H_{in} in function of Ca_{mag}, where χ is related with H_{in} through $\chi = \langle M \rangle / \beta H_{in}$, due to the fact that magnetic field inside the droplet is almost uniform. Here we observe that H_{in} is just a bit lower than one in low Ca_{mag}, where the magnetization is almost zero. It decreases as long as Ca_{mag} increases due to the fast growth of the magnetization in the Langevin linear region. It attains a minimum value at $Ca_{mag} \approx 2$ where the droplet starts to elongate, reducing the demagnetization geometrical factor, and increases with further increase in Ca_{mag}. This effect is coupled with χ causing a non-monotonic behavior, as pointed out just above.

The non-monotonic behavior of the magnetic permeability of magnetic emulsions was already observed in the experimental work of Ivanov and Kuznetsova (2012). Here, we should expect the same with $\langle M \rangle$ plotted in Fig. (2) because it is already scaled by H_0, so it represents the system or emulsion susceptibility. This behavior, however, does not happen because the non-dimensionalization and parameters used in this work retain neither a constant M_s nor a constant initial susceptibility χ_0 throughout the simulations.

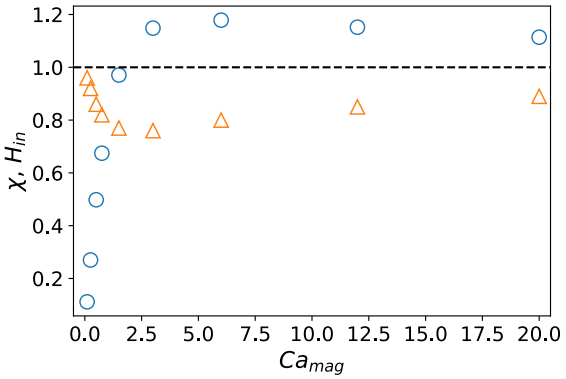

Figure 4. χ (blue circles) and H_{in} (orange triangles) in function of Ca_{mag} for the equilibrium case. The dashed line in χ, H_{in} equal to one is also included.

4.2 Non-equilibrium regime

Now we consider a non-equilibrium magnetization regime. For this analysis we set the same value for the non-dimensional saturation magnetization $M_s = \phi_f M_d = 1.0$ of the equilibrium case, with $\phi_f = 0.2$ and $M_d = 5$, and set $Ca_{mag} = 10$. These values have been chosen in order to maintain the Langevin function near the saturation region. The external magnetic field is applied in the x-direction. The present analysis consists of varying Ca and Pe_m, which correspond respectively to varying the vorticity inside the droplet and the magnetic relaxation time scale, respectively.

Figure 5 (a) shows θ, the arithmetic average of the local angles between $\mathbf{H}$ and $\mathbf{M}$ in the intersection between the XY-plane and the region inside the droplet, in function of Pe_m for $Ca = 0.1, 0.15$ and 0.2. As expected, θ depends mainly on Ca. This happens due to the different levels of vorticity induced inside the droplet so that the misalignment

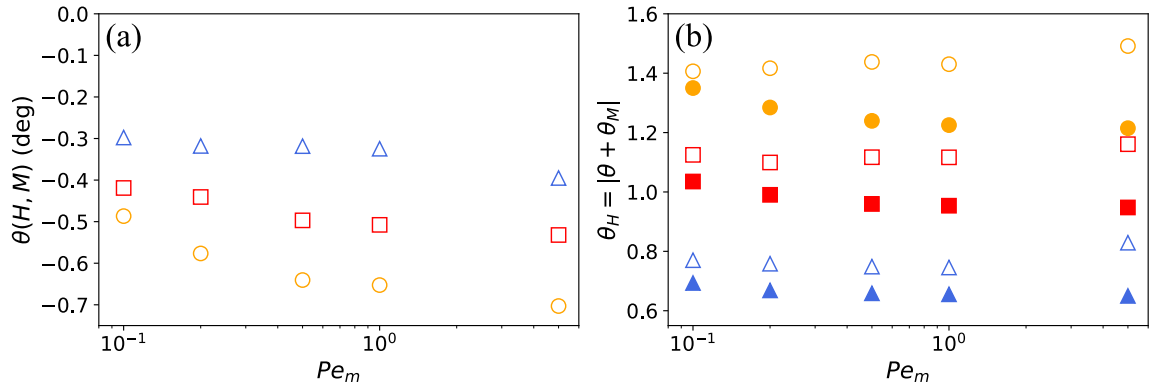

Figure 5. Averaged of local magnetic misalignment angles θ (a) and internal magnetic field angle θ_H (b) in function of Pe_m for $Ca = 0.1$ (blue markers), $Ca = 0.15$ (red markers) and $Ca = 0.2$ (orange markers) in equilibrium (filled markers) and non-equilibrium (empty markers) regimes.

term in Eq. (12) is implicitly larger as long as Ca increases and due to the coefficient Ca_{mag}/Ca (the ratio between magnetic and shear forces) of the magnetic precession term which diminishes as long as Ca increases. The negative sign indicates that $\mathbf{M}$ rotates in the direction of the vorticity, as expected. As shown in the graph, the increase in Pe_m also causes an increase in θ, which is in agreement with its definition: larger Pe_m means a smaller flow time scale. The local misalignment θ induces intrinsic torques in the fluid, leading to asymmetric stress states. In the interval observed in the present work, an angle of $\theta = 0.7$ is reached for $Ca = 0.2$ and $Pe = 5$. Figure 7 shows the spatial variation of the local misalignment angles together with the distribution of vorticity for that case. This angle is of the same order as the angle between the bulk magnetization and the applied magnetic field, θ_M, so the torque present in the system (or equivalent emulsion) due to θ_M (Cunha *et al.*, 2020; Abicalil *et al.*, 2021) should be of the same order the torques caused by the local misalignments. This could be an interesting result for studies of magnetic emulsions.

It is worth noting that with the non-dimensionalization process adopted here, the increase in Pe_m also increases the equilibrium magnetization $\mathbf{M_0}$. As a consequence, θ_M should decrease as long as Pe_m increases, in the absence of the vorticity effect on the magnetization, due to a more pronounced magnetization. The effect of the magnetic intensity on the bulk magnetization angle with the applied magnetic field direction is well explained in Abicalil *et al.* (2021). Fig. (5) (b) shows the angle $\theta_H = \theta_M + \theta$, which means approximately the angle between $\mathbf{H_{in}}$ and $\mathbf{H_0}$, in function of Pe_m for the three values of Ca with both approaches: considering the non-equilibrium regime (empty markers) and considering only the Langevin nature (filled markers). For the latter approach, the equilibrium one, the angle decreases as long as Pe_m decreases, as expected. These curves serve as parameters for the non-equilibrium cases. In these cases we observe a different trend, θ_H remains almost constant for $Pe_m \leq 1$ and increases with further increase in Pe_m, causing a crescent difference between the non-equilibrium and equilibrium cases, for all tested Ca.

In the case of non-equilibrium, the magnitude of the bulk magnetization $\langle M \rangle$ faces a non-monotonic behavior with respect to Pe_m, see Fig. (6). This happens possibly due to the increase of variability of the local misalignment angles in different droplet's regions given that there are regions with opposite signs in vorticity although the external simple shear flow induces a unidirectional vortex inside the droplet (see Fig. (7)). Despite the fact of lower bulk magnetization in the non-equilibrium regime, the local misalignment caused by the vorticity seems to improve the deformation of the droplet at smalls Pe_m with respect to the equilibrium regime, as shown in Fig. (6 b).

5. CONCLUSIONS

The approach used to integrate explicitly the magnetization evolution is good for computing the magnetization of a Langevin responsive ferrofluid droplet, although it requires smaller time steps than the ζ implicit approach. This implementation, then, is validated from the numerical point of view and can be used in non-equilibrium situations. As seen, two effects influence the bulk magnetization of a ferrofluid droplet under a uniform external field, the Langevin dynamics and the demagnetization caused by its elongation, being the first and the most important. A non-monotonic behavior of the magnetic susceptibility of the ferrofluid with respect to Ca_{mag} was observed.

When the vorticity has enough intensity to rotate the magnetization, we observed that it could influence significantly the deformation of the droplet and the bulk magnetization intensity. The local angles of misalignment between the magnetization and local magnetic field inside the droplet could attain levels comparable to those encountered between the bulk magnetization and the applied magnetic field, inducing important torques.

For future works, a non-dimensionalization M_s as a magnetic scale could be a good alternative for non-equilibrium and Langevin analysis of ferrofluid droplets.

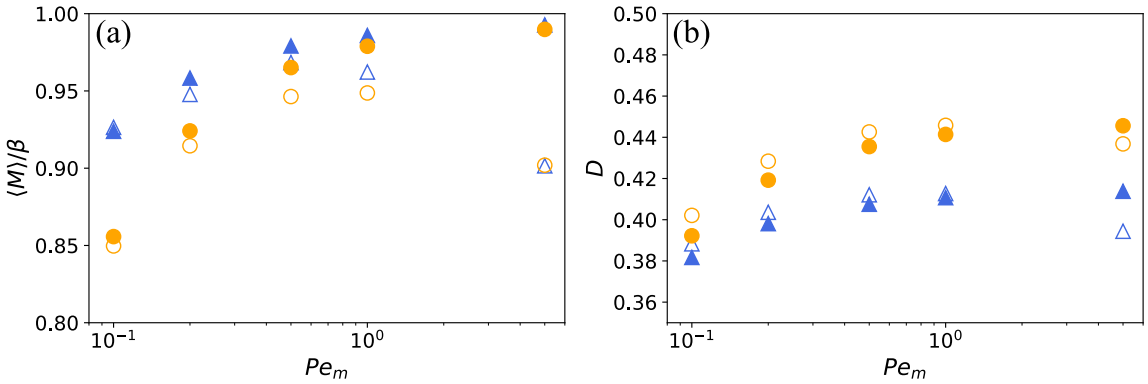

Figure 6. Bulk magnetization normalized by the droplet volume fraction β (a) and Taylor deformation D (b) in function of Pe_m for $Ca = 0.1$ (blue markers) and $Ca = 0.2$ (orange markers) in equilibrium (filled markers) and non-equilibrium (empty markers) regimes.

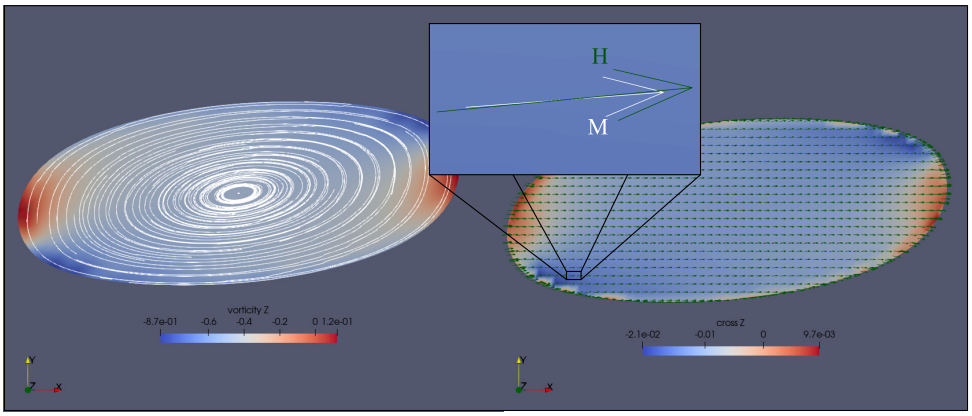

Figure 7. Slice in XY-plane of the droplet inside. On the left it is colored by the vorticity intensity in the z-direction together with streamlines. On the right, it is colored by the cross product between $\mathbf{H}$ and $\mathbf{M}$. The case for $M_d = 5$, $\phi_f = 0.2$, $Ca_{mag} = 10$, $Ca = 0.2$ and $Pe_m = 5$.

From the numerical perspective, more robust hyperbolic evolution algorithms need to be implemented in order to guarantee stability with greater time steps. Also more accurate equations for the magnetization evolution in high non-equilibrium situations should be tested, as these described in (Shliomis, 2001), together with an equation for the equilibrium magnetization that accounts for the dipole interactions (Ivanov and Kuznetsova, 2001).

6. ACKNOWLEDGEMENTS

This research was supported by CNPq (Ministry of Science, Technology, and Innovation of Brazil) under grants 131422/2021-9 (A.L.G.) and 310631/2021-1 (T.F.O.).

7. REFERENCES

Abicalil, V.G.e., Abdo, R.F., da Cunha, L.H.P. and de Oliveira, T.F., 2021. "On the magnetization of dilute ferrofluid emulsions in shear flows". *Physics of Fluids*, Vol. 33, No. 5, p. 053313.

Afkhami, S.a., Tyler, A., Renardy, Y., Renardy, M., Pierre, T.S., Woodward, R. and Riffle, J.S., 2010. "Deformation of a hydrophobic ferrofluid droplet suspended in a viscous medium under uniform magnetic fields". *Journal of Fluid Mechanics*, Vol. 663, pp. 358–384.

Capobianchi, P., Lappa, M., Oliveira, M.S. and Pinho, F.T., 2021. "Shear rheology of a dilute emulsion of ferrofluid droplets dispersed in a nonmagnetizable carrier fluid under the influence of a uniform magnetic field". *Journal of Rheology*, Vol. 65, No. 5, pp. 925–941.

Cunha, L., Siqueira, I., Cunha, F. and Oliveira, T., 2020. "Effects of external magnetic fields on the rheology and magnetization of dilute emulsions of ferrofluid droplets in shear flows". *Physics of Fluids*, Vol. 32, No. 7, p. 073306.

Cunha, L.H., Siqueira, I.R., Oliveira, T.F. and Ceniceros, H.D., 2018. "Field-induced control of ferrofluid emulsion rheology and droplet break-up in shear flows". *Physics of Fluids*, Vol. 30, No. 12, p. 122110.

de Carvalho, D.D. and Gontijo, R.G., 2020. "Magnetization diffusion in duct flow: The magnetic entrance length and the

interplay between hydrodynamic and magnetic timescales". *Physics of Fluids*, Vol. 32, No. 7, p. 072007.

Ishida, S. and Matsunaga, D., 2020. "Rheology of a dilute ferrofluid droplet suspension in shear flow: Viscosity and normal stress differences". *Physical Review Fluids*, Vol. 5, No. 12, p. 123603.

Ivanov, A.O. and Kuznetsova, O.B., 2001. "Magnetic properties of dense ferrofluids: An influence of interparticle correlations". *Physical Review E*, Vol. 64, No. 4, p. 041405.

Ivanov, A.O. and Kuznetsova, O.B., 2012. "Nonmonotonic field-dependent magnetic permeability of a paramagnetic ferrofluid emulsion". *Physical Review E*, Vol. 85, No. 4, p. 041405.

Jiang, G.S. and Peng, D., 2000. "Weighted eno schemes for hamilton–jacobi equations". *SIAM Journal on Scientific computing*, Vol. 21, No. 6, pp. 2126–2143.

Kim, J. and Moin, P., 1985. "Application of a fractional-step method to incompressible navier-stokes equations". *Journal of computational physics*, Vol. 59, No. 2, pp. 308–323.

Rosensweig, R.E., 2013. *Ferrohydrodynamics*. Courier Corporation.

Rowghanian, P., Meinhart, C. and Campàs, O., 2016. "Dynamics of ferrofluid drop deformations under spatially uniform magnetic fields". *Journal of Fluid Mechanics*, Vol. 802, pp. 245–262.

Shliomis, M.I., 2001. "Ferrohydrodynamics: Testing a third magnetization equation". *Physical Review E*, Vol. 64, No. 6, p. 060501.

Shliomis, M. *et al.*, 1971. "Effective viscosity of magnetic suspensions". *Zh. Eksp. Teor. Fiz*, Vol. 61, No. 2411, pp. s1971d–1971.

Sussman, M. and Fatemi, E., 1999. "An efficient, interface-preserving level set redistancing algorithm and its application to interfacial incompressible fluid flow". *SIAM Journal on scientific computing*, Vol. 20, No. 4, pp. 1165–1191.

Sussman, M., Fatemi, E., Smereka, P. and Osher, S., 1998. "An improved level set method for incompressible two-phase flows". *Computers & Fluids*, Vol. 27, No. 5-6, pp. 663–680.

Sussman, M., Smereka, P. and Osher, S., 1994. "A level set approach for computing solutions to incompressible two-phase flow". *Journal of Computational physics*, Vol. 114, No. 1, pp. 146–159.

Taylor, G.I., 1934. "The formation of emulsions in definable fields of flow". *Proceedings of the Royal Society of London. Series A, containing papers of a mathematical and physical character*, Vol. 146, No. 858, pp. 501–523.

Yang, W. and Liu, B., 2020. "Effects of magnetization relaxation in ferrofluid film flows under a uniform magnetic field". *Physics of Fluids*, Vol. 32, No. 6, p. 062003.

Zhu, G.P., Nguyen, N.T., Ramanujan, R.V. and Huang, X.Y., 2011. "Nonlinear deformation of a ferrofluid droplet in a uniform magnetic field". *Langmuir*, Vol. 27, No. 24, pp. 14834–14841.

8. RESPONSIBILITY NOTICE

The following text, properly adapted to the number of authors, must be included in the last section of the paper: The author(s) is (are) solely responsible for the printed material included in this paper.